Title

Fermi-level Dirac crossings in 4*d* and 5*d* cubic metal oxides: $NaPd_3O_4$ and $NaPt_3O_4$

Journal

Physical Review B, 99(19)

ISSN

2469-9950 2469-9969

Authors

Teicher, Samuel M. L
Lamontagne, Leo K
Schoop, Leslie M
et al.

Publication Date

2019-05-28

DOI

10.1103/PhysRevB.99.195148

Peer reviewed

Fermi level Dirac crossings in 4d and 5d cubic metal oxides: $NaPd_3O_4$ and $NaPt_3O_4$

Samuel M. L. Teicher[1], Leo K. Lamontagne[1], Leslie M. Schoop,[2] and Ram Seshadri[1]
[1]*Materials Department and Materials Research Laboratory, University of California, Santa Barbara 93106, USA and*
[2]*Department of Chemistry, Princeton University, Princeton 08540, USA**

The cubic oxide metals NaM_3O_4 (M = Pd or Pt) crystallize in the non-symmorphic $Pm\bar{3}n$ space group. First-principles calculations are employed here to understand the role of the MO_4 square planes and *M*–*M* interactions in the development of the electronic structure. The compounds host numerous Dirac crossings near the Fermi level which, in the absence of spin-orbit coupling, appear to form a cubic nodal state. Spin-orbit coupling fragments this nodal state into smaller regions with Dirac-like character, with the fragmenting being more pronounced in the the M = Pt compound.

I. INTRODUCTION

Dirac semimetals (DSMs) have become an active area of research due to their exceptional transport properties, arising as a consequence of a linear band crossing, or Dirac point, which results in massless charge carriers known as Dirac fermions. In order for the transport to be dominated by Dirac fermions, Dirac points in the electronic structure should be proximal to the Fermi level with few or no other bands at the same energy. DSMs could be considered 3D analogs of graphene, which is a 2D material with purely linear band crossings at the Fermi level.[1] There is an additional constraint on DSMs, however, that graphene does not satisfy, that the crossing must be symmetry-protected such that it does not gap out due to spin-orbit coupling (SOC) and or an applied magnetic field.[2] In recent years, a push to develop design principles for 3D DSMs that possess these protected linear band crossings near the Fermi level has yielded the experimental verification compounds Na_3Bi and Cd_3As_2.[3–6] A closely related class of materials to DSMs have degenerate Dirac crossings along a line in the Brillouin zone, rather than points and these are called nodal-line semimetals.[7–9] SOC is often unfavorable for the formation of these features in the electronic structure since symmetry protections tend to only exist along high-symmetry lines in k-space, and thus do not usually fully stabilize the nodal lines, which are frequently circular or oval.[10] Nodal-line semimetals with certain symmetry protections exhibit drumhead-shaped surface states that are proposed to host novel correlated electron physics.[9] Recently, it has been proposed that rather than displaying nodal lines, there could exist compounds in which the degenerate band crossings trace a connected 3D surface — a spherical shell — in the Brillouin zone,[11] these nodal-sphere semimetals could exhibit similar correlated surface states.

Analyzing and understanding crystallographic and compositional motifs that lead to linear band crossings proximal to the Fermi level is important in identifying new compounds and advancing potential technological applications. It is also of particular interest to examine oxide compounds which are somewhat underrepresented in the space of Dirac and related materials. To this end, we present electronic structure calculations on the complex platinum group metal oxides, NaM_3O_4 (M = Pd, Pt). Since the strength of SOC scales approximately as Z^4/n^3, (Z is the atomic number and n is the principal quantum number) comparing the Pd and Pt compounds allows the role of SOC in the development of the electronic structure to be scrutinized.

From the perspective of current applications, these complex Pd and Pt oxides are known for their their ability to be p-doped. Unlike most oxides which have valence bands dominated by localized O p orbitals and are most conveniently electron doped, these Pd and Pt compounds can be easily hole-doped using alkali metals.[12,13] The semiconducting d^8 oxides (Ca/Sr)(Pd/Pt)$_3O_4$ can be hole doped by Na substitution for Ca/Sr. Substitution on this site does not significantly change the crystal structure or the qualitative nature of bands, allowing fine tuning of the Fermi level. Sodium doping of CaM_3O_4 and SrM_3O_4 has been shown to convert these semiconductors into metals.[14–17] NaM_3O_4 can be viewed as the 100%-doped end-member in which Ca or Sr has been completely replaced by Na. Lamontagne *et al.* recently proposed that Na doping in $CaPd_3O_4$ and $SrPd_3O_4$ may proceed *via* a non-uniform percolative transition, with significantly increased local disorder in $SrPd_3O_4$ impeding percolation relative to $CaPd_3O_4$.[18]

Platinum metal has also long been ubiquitous as a chemical catalyst, and Pd oxides are well-known for their use in automotive catalytic converters. In the 1970s, $Na_xPt_3O_4$ was proposed to be one of the main active components of the Adams catalyst, a compound useful for catalyzing organic hydrogenation reactions that was first described by Adams and Voorhees in 1922, whose properties proved difficult to reproduce over a half-century of subsequent syntheses.[19,20] In recent years, there has been significant general interest in the enhanced catalytic action of ionic noble metal species and noble metal oxides.[21–24] It is interesting to ask whether topological surface states and/or potentially enhanced charge transport due to linear dispersion at Dirac and Weyl band crossings could play a role in the catalytic activity of these compounds. Indeed, a growing number of catalysts including the pure noble metals Pd and Pt, have been suggested as hosting non-trivial topolog-

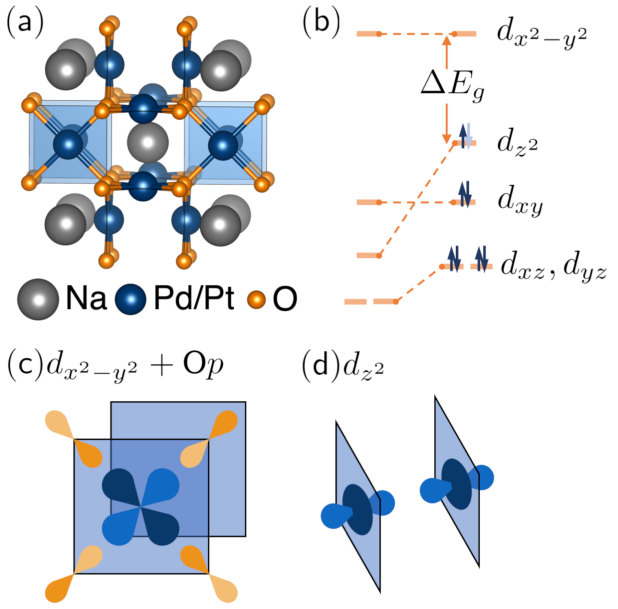

FIG. 1. (a) Crystal structure of Na(Pd/Pt)$_3$O$_4$ in the nonsymmorphic space group $Pm\bar{3}n$ (#223). (b) Crystal field splitting for the general square planar case, modified here through the interaction between the partially filled d_{z^2} levels across the faces of the square planes. The energy gap for the corresponding d^8 compounds would be between the d_{z^2} and $d_{x^2-y^2}$ levels. For (Ca/Sr)M_3O$_4$, the d_{z^2} states are filled, resulting in a band insulator. For NaM_3O$_4$, however, the d_{z^2} states are partially filled, resulting in a metal. (c) The $d_{x^2-y^2}$ + O p interaction for a single square plane. (d) The stacked MO$_4$ square planes in the unit cell yield a network of inter-planar $M_{d_z^2}$ bonding.

ical states and linear band crossings in their electronic structure.[25,26]

NaPd$_3$O$_4$ and NaPt$_3$O$_4$ crystallize in the cubic $Pm\bar{3}n$ space group (#223) shown in Fig. 1(a). The structure consists of corner-connected MO$_4$ square planes. Closely-spaced, infinite parallel stacks of MO$_4$ square planes also run along all three cubic axes. The space group has an n glide that results in nonsymmorphic symmetry. Recently, there has been significant interest in 3D nonsymmorphic crystals, especially due to the fact that these compounds can host protected multiply-degenerate band crossings in which more than 4 bands overlap at high-symmetry points in the Brillouin zone. At these overlap points, even more exotic analogs of Dirac fermions could potentially be realized.[27–29] Group #223 can host band crossings that are up to eight-fold degenerate.[29]

The crystal-field splitting of square planar M as presented in Fig. 1(b), has been described using tight binding models as popularized by Hoffmann[30] and an important feature is that interaction of the d_{z^2} orbitals raises this level over the d_{xy} level as shown in the right. The $d_{x^2-y^2}$ orbitals form a 3D-connected bonding network with the O p orbitals at the corner of each square planar group [Fig. 1(c)]. The d_{z^2} orbitals form independent bonding chains with two square planar groups *per* unit cell along the cubic axes [Fig. 1(d)]. 3D bonding increases the energy dispersion of the $d_{x^2-y^2}$ bands (which would not be expected to have particularly significant dispersion in the isolated chain model), allowing them to cross the d_{z^2} bands near the center of the Brillouin zone, and, as will be shown, resulting in symmetry-protected Dirac crossings. Doublet, Canadell, and Whangbo have developed a semi-empirical tight-binding model for NaM_3O$_4$ and provided band-folding explanations for the electronic structure of the $d_{x^2-y^2}$ and d_z^2 states near the Fermi-level.[31] The Pd/Pt ions in NaM_3O$_4$ have a nominal 2.33+ charge, making these compounds metallic with partially-filled d_z^2 orbitals. This is in contrast to the isostructural, band semiconducting compounds with Ca or Sr which have d^8 Pd^{2+} or Pt^{2+} and a fully-filled d_z^2 level. The compounds (Ca/Sr)M_3O$_4$ have previously been suggested to be topological semimetals, but these compounds are actually insulating both at appropriate levels of electronic structure theory as well as in experimental studies.[18,32]

We present here a detailed electronic structure description of the two compounds NaPd$_3$O$_4$ and NaPt$_3$O$_4$ using a combination of plane-wave pseudopotential and plane-wave local orbital density functional theory calculations in tandem with tight-binding models to identify Dirac crossings near the Fermi level that appear to form a nodal cube, not unlike the nodal-sphere semimetallic state proposed previously by Wang *et al.*[11] Spin-orbit coupling fragments this nodal cubic state into 14 protected Dirac crossings in both the Pd and Pt compounds. This work points to the potential of complex oxides to enrich the domain of Dirac and related quantum materials and supports the view that there may be a role for previously ignored features in the electronic structure playing a role in the catalytic properties of compounds of the platinum group metals.

II. COMPUTATIONAL METHODS

First principles electronic structure calculations were performed using Vienna ab initio Simulation Package VASP[33–35] and WIEN2k codes,[36] with and without SOC. Computation performed using VASP utilized projector-augmented waves,[37,38] while computations involving WIEN2k employed linear augmented plane waves and local orbitals.[39] The Perdew, Burke, Ernzerhof (PBE) generalized gradient approximation[40] was used for the exchange energy while Vosko, Wilk, and Nusair interpolation was used for the correlation energy.[41] While computationally expensive hybrid functionals such as HSE06,[42] are known to improve band gap estimations in a wide range of semiconductors, including in simple and complex Pd oxides,[43] previous empirical comparisons of transition metal and metallic transition metal oxide systems suggest that the additional electron screening in hybrid functionals provides little improvement

over PBE and can reduce accuracy in estimations of key material parameters.[44,45] We employed a $10 \times 10 \times 10$ Monkhorst-Pack[46] k-point grid. Structural relaxations and static self-consistent calculations used the default smearing algorithms for VASP and WIEN2k, first-order Methfessel-Paxton[47] and tetrahedral smearing with Blöchl corrections,[48] respectively. The plane wave energy cutoff for VASP was set to 520 eV and the plane-wave expansion parameter, RKMAX, for WIEN2k was set to 8.5. The density of states calculations provided in the supplemental material utilized tetrahedral smearing and band structures were calculated using Gaussian smearing.[49] Structures were initially relaxed in VASP (to lattice parameters of 5.728 Å and 5.765 Å for the the Pd and Pt compounds, respectively, within expected error from experimental values of 5.650 Å[50] and 5.689 Å[51]) using the conjugate gradient descent algorithm with a force cutoff of 0.01 eV/Å. Self-consistent static calculations and electronic structure calculations were subsequently performed using VASP and WIEN2k with energy convergence better than 10^{-5} eV.

Brillouin zone energy gap calculations on the $k_z = 0$ plane were calculated in VASP using a $30 \times 30 \times 1$ k-mesh and Gaussian smearing. Orbital-projected band structures were calculated using WIEN2k without SOC but were checked against results from VASP and a spin-polarized WIEN2k calculation with SOC. The charge density of valence electrons contributing to energy states within 0.1 eV of the Fermi level was computed using WIEN2k. Irreducible representations of electronic bands were determined using the IRREP subprogram in WIEN2k. The Brillouin zone Dirac crossing calculations were performed by projecting our VASP calculations onto maximally localized Wannier functions using Wannier90,[52] starting from initial projectors corresponding to valence orbitals (Na s and p; Pd/Pt s,p, and d; O s and p), constructing a tight-binding model from these localized Wannier functions, and subsequently using the GAPPLANE and GAPCUBE functions in the Wannier Tools package[53] with 400×400 and $200 \times 200 \times 200$ sampling meshes, respectively. The tight-binding models are very slightly asymmetrical with respect to the cubic crystalline structure; this is a result of Wannier90's Wannier function localization algorithm rather than inherent asymmetry in the original DFT simulation. Structures were visualized with VESTA.[54]

III. RESULTS AND DISCUSSION

The electronic band structures of $NaPt_3O_4$ and $NaPd_3O_4$ with and without the inclusion of SOC are given in Fig. 2. We focus our attention on the bands near the Fermi level from the Γ to X high symmetry points. These bands cross just below the Fermi level with a large linear energy dispersion that is as great as 0.5 eV in $NaPt_3O_4$. Viewing along the $M-\Gamma$ and $\Gamma-R$ branches, additional, smaller linear band crossings can be seen. A

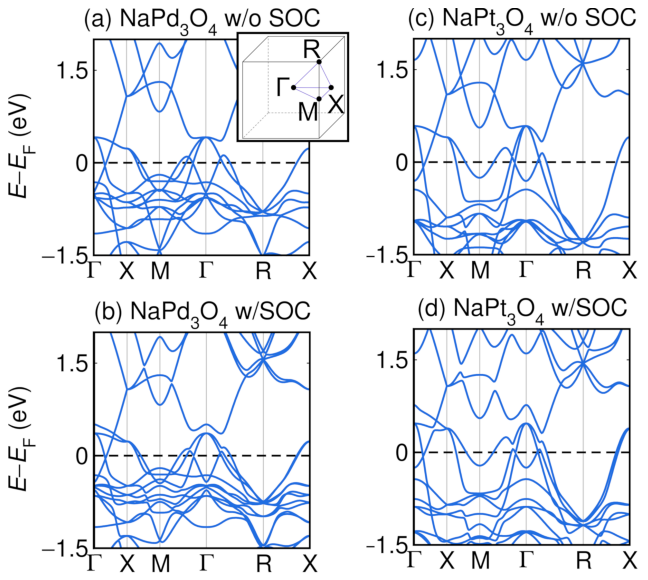

FIG. 2. Band structures of $NaPd_3O_4$ (a) without and (b) with SOC and $NaPt_3O_4$ (c) without and (d) with SOC calculated using the PBE functional in VASP. A linear band crossing near the Fermi level is evident in the $\Gamma - X$ direction with large energy dispersion (≈ 0.5 eV). Smaller linear band crossings occur along $M - \Gamma$ and $\Gamma - R$.

close-up view of the band crossings is provided in Fig. 3. The Dirac crossings along $\Gamma - X$ and $\Gamma - R$ are symmetry-protected, while the $M - \Gamma$ crossing is gapped out when SOC is included. Calculations in VASP and WIEN2k show good agreement for states above the Fermi level and in the Fermi level region where the Dirac crossings lie. Predicted energies for states below the Fermi level differ slightly for the two methods. This is unsurprising given the local orbital approach in WIEN2k. Although WIEN2k calculations are not shown in Fig. 2 for the sake of visual clarity, a direct comparison of the band structures calculated in both codes is available in the supplementary information.[49]

Nonsymmorphic symmetry protects multiply-degenerate band crossings in both materials. Eight-fold crossings can be seen at energies near 1.5 eV and between -0.6 eV and -1.5 eV at the R point, the energy of the latter, sub-Fermi level degeneracy varying significantly with M site species and simulation program. While the eight-fold crossings are very far from the Fermi level in these compounds, they are relevant to electronic structure of closely-related compounds. It has been shown that the Fermi level of the isostructural compound $LaPd_3S_4$ lies near the upper eight-fold degeneracy at R and Pt_3O_4 appears to have a Fermi level near the lower eight-fold degeneracy.[29]

In order to explore the origins of the Fermi level Dirac crossings, we consider symmetry and orbital character. Formally, symmetry protects band crossings from gapping if the two crossing bands have different irreducible

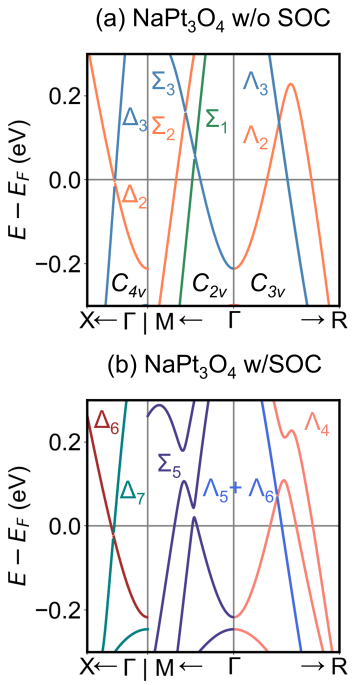

FIG. 3. Close-up views of the Dirac cones along the $\Gamma - X$, $M - \Gamma$, and $\Gamma - R$ paths of the band structures of $NaPt_3O_4$ (a) without and (b) with SOC calculated in WIEN2k. The Dirac cones along $M - \Gamma$ are gapped by SOC whereas the other Dirac cones are protected in both compounds. Colors of the plotted bands represent calculated irreducible representations (irreps).

representations (irreps) with respect to the point group of the k-vector.[10] When SOC is significant, the two band irreps must be different with respect to the double group, which accounts for spin. The gapping of the Dirac crossing along $M - \Gamma$ when SOC is introduced can be explained as a consequence of the cubic space group. The $\Gamma - X$, $M - \Gamma$ and $\Gamma - R$ lines in k-space obey C_{4v}, C_{2v}, and C_{3v} point group symmetries, respectively. Without SOC, the crossing bands have different irreps in each of these point groups and all three crossings are allowed (See the irrep-colored bands of Fig. 3). When SOC is introduced, there is only one spinor irrep available in the double group of C_{2v} and the Dirac crossing along $M - \Gamma$ therefore gaps out. Explicitly, we calculate the irreps of the crossing bands along the three high-symmetry Brillouin zone lines in the system with SOC: $\Gamma - X$: $\{\Delta_6, \Delta_7\} \rightarrow \{\Delta_7, \Delta_6\}$; $M - \Gamma$: $\{\Sigma_5, \Sigma_5\} \rightarrow \{\Sigma_5, \Sigma_5\}$; $\Gamma - R$: $\{\Lambda_4, \Lambda_5 + \Lambda_6\} \rightarrow \{\Lambda_5 + \Lambda_6, \Lambda_4\}$.[55] The irreps are identical for both the Pd and Pt compounds. There is an exchange of irreps at the $\Gamma - X$ and $\Gamma - R$ crossings, and these crossings are therefore protected, while no such exchange can occur along $M - \Gamma$. More specifically, the Dirac crossings along $\Gamma - X$ and $\Gamma - R$ are protected by C_4 and C_3 rotational symmetry, respectively, as the irreps of the crossing bands at these points are distinguished by their character with respect to these symmetry operations. Overall, we can state that the symmetry protections in the system are completely general properties of the cubic Brillouin zone and can be extended to cubic compounds in other space groups.

Figure 4 presents orbital-projected band structures and a visualization of the valence electron charge distribution contributing to energy states near the Fermi level in NaM_3O_4. The difference in symmetry between the bands crossing at the Dirac cones can be seen to reflect a difference in orbital origin. The dominant contributions are from M $d_{x^2-y^2}$ and d_{z^2} orbitals in tandem with O (mainly p) states. Density of states calculations supporting this conclusion are also offered in the supplement.[49] The Dirac crossings are created by the overlap of partially-filled d_{z^2} bands with large-dispersion $d_{x^2-y^2}$ bands that dip down in energy at Γ. Oxygen states overlap significantly with both orbitals, but interact more strongly with the $d_{x^2-y^2}$ band. It is important to note here that we are using a local bonding basis to describe the the states, rather than the crystal coordinates, such that $d_{x^2-y^2}$ refers to an M orbital with lobes pointing along the square planar coordinated bonds towards oxygen. Although the orbital decomposition generally follows the energy level diagram of Fig. 1(c), the non-negligible interaction of oxygen states with the d_{z^2} might be somewhat unexpected. Figure 4 (e,f) show that the O p orbitals are oriented along $[111]$ axes, facing out of the square coordination plane defined by M-O bonding such that they can interact with additional orbitals along the z-axis. The Pd compound has more disperse orbitals than the Pt compound and has less directional d orbital preference along the Pd-O bonds (the Pd d orbitals have more d_{xy} character in addition to the primary $d_{x^2-y^2}$, d_{z^2} character).

From the perspective of simulation, all three Dirac crossings of interest occur between the same two bands. Since the system is metallic, there is no good division between "valence" and "conduction" bands, we refer to the band with greater energy at the Γ point, which descends in energy towards the Dirac crossings along Γ-X, Γ-M, and Γ-R, as the "B_+" band, while the band with lower energy at Γ will be referred to as "B_-." These simulation-defined bands are visualized in Fig. 4(d). While this scheme is sufficient for our purposes, note that the Γ-R Dirac cone is actually 6-fold degenerate (composed of 3 separate sets of spin-degenerate bands) in the non-SOC calculations, though this degeneracy is gapped by SOC.

Figure 5 shows the energy landscape of the B_- and B_+ bands along a constant $k_z = 0$ slice in the (cubic) Brillouin zone for $NaPt_3O_4$. As discussed by Doublet *et al.*, the roughly square shape of the Fermi surface of the d_{z^2} band can be viewed as a consequence of the relative independence of the MO_4 bonding chains along x and y.[31] Despite the 3D connectivity of the M $d_{x^2-y^2}$+ O p bonding network, the corresponding Fermi surface is roughly square as well. The net result is that both the B_- and B_+ bands have cubic symmetry. There are two regions where these bands come close together: along a square loop at the center of the Brillouin zone, corresponding to the Dirac crossings, and, far below the Fermi level, along

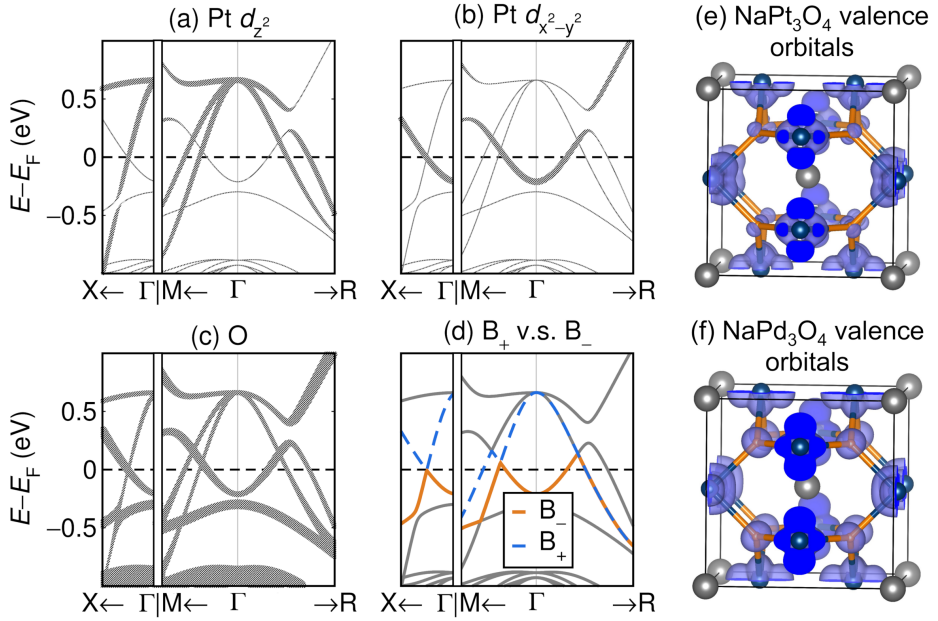

FIG. 4. Determination of orbital character. (a)-(c): orbital projected band structures of $NaPt_3O_4$ calculated in WIEN2k. Dirac cones are generated by the crossing of M d_{z^2} and M $d_{x^2-y^2}$ bands. (d): the same plot with an overlay of the simulation-defined bands B_+ and B_- that form the tops and bottoms of the Dirac crossings, respectively. These bands will be further visualized in Fig. 5 and Fig. 6. (e,f): Charge density of valence states contributing to bands within 0.1 eV of the Fermi level in $NaPt_3O_4$ and $NaPd_3O_4$, respectively, suggesting primary contributions from Pt $d_{x^2-y^2}$ and d_{z^2} orbitals in combination with O p orbitals. The charge density is visualized at a constant contour of $0.0021\, e^-$ Å^{-3}.

the $\Gamma - M$ line from the center of the diagram to the corners.

In order to achieve a higher k-space sampling resolution to more precisely visualize the locations of the Dirac crossings, we implemented Wannier-interpolated tight-binding models as discussed in section II. Figure 6 shows calculations of the energy gaps in the area of the Brillouin zone near the central square intersection region of Fig. 5. (a) and (b) demonstrate that there is a full square nodal line in the $k_z = 0$ plane that is interrupted by gapping along $\Gamma - M$ when SOC is introduced. (c) and (d) show that the nodal square in the Pd compound without SOC is part of a larger small energy-splitting region with roughly cubic shape, but small holes in the nodal cube, which SOC gaps into eight protected degeneracies along $\Gamma - R$ and six protected degeneracies along $\Gamma - X$ for a total of 14 Dirac points. The $\Gamma - R$ crossings have sharp dispersion whereas the $\Gamma - X$ Dirac crossings have very small dispersion along the faces of the cube and appear flat and plate-like even after SOC is included. The nodal cube in $NaPt_3O_4$ in the absence of SOC is found to be a complete cube, (e), similar to a nodal sphere semimetal. More generally, the cubic degeneracy region in the Pt compound is noticeably more square than the similar region in the Pd compound and the stronger SOC in this compound more fully removes the nodal cube degeneracy, although small, plate-like dispersion along $\Gamma - X$ remains (see supplement for $k_z = 0$ plane nodal lines in $NaPt_3O_4$).[49] At the smallest energy splittings available in our tight-binding models, the intersection region in the Pd compound is reduced to a number of nodal lines. The Pt compound, by contrast, has a full, nodal-cubic Dirac degeneracy in the absence of SOC down to the lowest reasonable simulation energies (see supplement).[49] These qualitative findings were found to be robust to re-parameterization of the tight-binding model using a number of alternative orbital projections, including a model including only the M $d_{x^2-y^2}$, d_{z^2} and O p orbitals previously discussed.

IV. CONCLUSIONS

We have shown that the high symmetry structures of NaM_3O_4 result in the formation of 14 Fermi level Dirac crossings that are protected against spin-orbit coupling, with a particularly large linear energy dispersion region about $\Gamma - X$. These compounds can potentially be doped between interesting electronic states including the nonsymmorphic-symmetry-enabled degenerate R point bands of M_3O_4, the Dirac cones of NaM_3O_4 discussed, and the insulating compounds (Ca/Sr)M_3O_4.

The $Pm\bar{3}n$ cubic space group appears promising for the generation of a stable nodal cube state with surface states that could host exciting correlated electron physics.[11] While the compounds discussed here have significant SOC that prevents the realization of a true nodal cube, this state might be achieved in related systems by

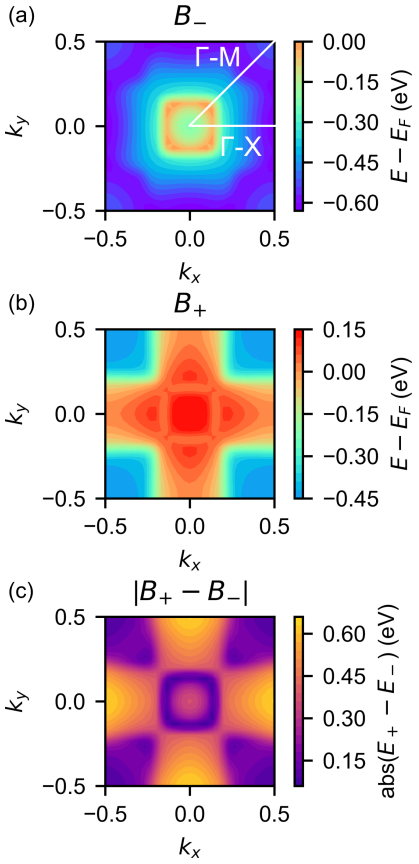

FIG. 5. Heatmaps of band energies on the $k_z = 0$ plane. Energies of the B_- and B_+ bands are shown for $NaPt_3O_4$ with SOC. The absolute value of the energy separation between the B_- and B_+ bands is shown in (c). The Fermi-level Dirac crossings between the B_- and B_+ comprise an approximately square energy degeneracy loop in the region $\{-0.2 \leq k_x \leq 0.2; -0.2 \leq k_y \leq 0.2\}$.

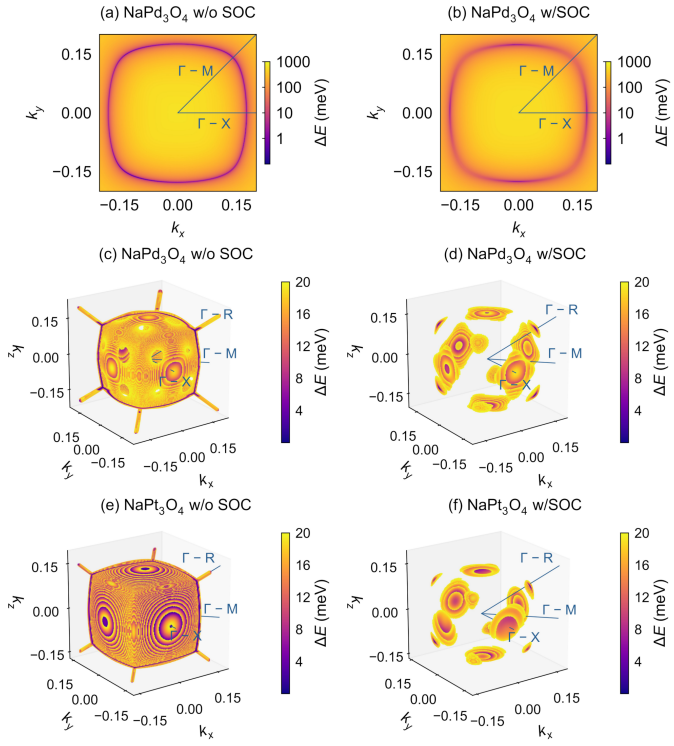

FIG. 6. High-resolution calculations of energy-splitting between NaM_3O_4 B_+/B_- bands in k-space, performed with tight-binding model: 2D plots in (a) and (b) show all energies on a logarithmic scale, while for 3D plots in (c-f) the maximum energy cutoff was 20 meV.

lowering SOC using lighter elements. The presence of a full nodal cube in the Pt compound without SOC also gives us some hints as to how we might go about creating such a state in a real material. The cubic Dirac degeneracy of these compounds is a direct consequence of the quasi-independence of the MO_4 square-planar bonding chains in the unit cell. The d_{z^2} bonding network is nearly independent along the cubic axes resulting in a B_+ band that creates the nodal cubic state [Fig 5(a)]. Dirac character along the $\Gamma - X$ direction is directed towards the cubic faces of the (001) single crystal surface with metallic or mixed Dirac-metallic character along other high-symmetry directions. Interaction with the ligand oxygens increases the 3D connectivity of the $d_{x^2-y^2}$ bonding network and reduces the how cubic the Dirac crossings are. In the absence of SOC, increased Pd-O bonding in the Pd compound compared to the Pt-O bonding of the Pt compound results in a less perfect nodal cube degeneracy. A possible way to reduce the M-O bonding would be to increase the lattice parameter though chemical strain, for example though substituting K^+ or Rb^+ for Na^+.

Effects of these predicted Fermi level Dirac crossings and large k-space regions of linear dispersion may be detectable in magnetotransport measurements. A number of compounds in this family, including $Na_xPt_3O_4$, have been previously synthesized as single crystals suitable for transport studies.[56–59] Nodal-line semimetals frequently show signs of anomalous transport such as large magnetoresistance and low-field quantum oscillations.[60,61]

The band inversion in this system results from bonding chains, rather than the relativistic contraction of s orbitals on a single atomic site (as in the now-canonical DSM examples Na_3Bi and Cd_3As_2), so this compound can be classified with other new "molecular" semimetals such as ZrSiS that feature large linear energy dispersion.[62]

The significance of the transport contribution from linear bands to catalysis has not yet been fully deciphered. Nonetheless, Dirac transport in NaM_3O_4 may further our understanding of the Adams catalyst on the centennial of its discovery. While topological semimetals have been previously examined as catalysts for the hydrogen evolution reaction, hydrogenation catalysts may also prove a fruitful avenue of inquiry.

ACKNOWLEDGMENTS

We thank Claudia Felser for encouraging this work, and Douglas Fabini and Xie Zhang for helpful discussions. This work was supported by the National Science Foundation through DMR 1710638. Initial support to SMLT from a New Partnerships Challenge Grant program of the California Nanosystems Institute (CNSI) is gratefully acknowledged. LMS was supported by the Princeton Center for Complex Materials, a Materials Research Science and Engineering Center (MRSEC) DMR-1420541, and by the Princeton Catalysis Initiative (PCI). We gratefully acknowledge the use of the computing facilities of the Center for Scientific Computing at UC Santa Barbara, supported by NSF CNS-1725797 and by the NSF MRSEC Program (NSF DMR-1720256). SMLT has been supported by the National Science Foundation Graduate Research Fellowship Program under Grant No. DGE-1650114. Any opinions, findings, and conclusions or recommendations expressed in this material are those of the authors and do not necessarily reflect the views of the National Science Foundation.

* steicher@ucsb.edu,lschoop@princeton.edu

[1] A. H. Castro Neto, F. Guinea, N. M. R. Peres, K. S. Novoselov, and A. K. Geim, Rev. Mod. Phys. **81**, 109 (2009).
[2] N. P. Armitage, E. J. Mele, and A. Vishwanath, Rev. Mod. Phys. **90**, 015001 (2018).
[3] Q. D. Gibson, L. M. Schoop, L. Muechler, L. S. Xie, M. Hirschberger, N. P. Ong, R. Car, and R. J. Cava, Phys. Rev. B **91**, 205128 (2015).
[4] B.-J. Yang and N. Nagaosa, Nat. Commun. **5**, 4898 (2014).
[5] Z. K. Liu, B. Zhou, Y. Zhang, Z. J. Wang, H. M. Weng, D. Prabhakaran, S.-K. Mo, Z. X. Shen, Z. Fang, X. Dai, Z. Hussain, and Y. L. Chen, Science **343**, 864 (2014).
[6] Z. K. Liu, J. Jiang, B. Zhou, Z. J. Wang, Y. Zhang, H. M. Weng, D. Prabhakaran, S.-K. Mo, H. Peng, P. Dudin, T. Kim, M. Hoesch, Z. Fang, X. Dai, Z. X. Shen, D. L. Feng, Z. Hussain, and Y. L. Chen, Nat. Mater. **13**, 677 (2014).
[7] C. Fang, Y. Chen, H.-Y. Kee, and L. Fu, Phys. Rev. B **92**, 081201 (2015).
[8] L. S. Xie, L. M. Schoop, E. M. Seibel, Q. D. Gibson, W. Xie, and R. J. Cava, APL Mater. **3**, 083602 (2015).
[9] Y.-H. Chan, C.-K. Chiu, M. Y. Chou, and A. P. Schnyder, Phys. Rev. B **93**, 205132 (2016).
[10] L. M. Schoop, F. Pielnhofer, and B. V. Lotsch, Chem. Mater. **30**, 3155 (2018).
[11] J. Wang, Y. Liu, K.-H. Jin, X. Sui, L. Zhang, W. Duan, F. Liu, and B. Huang, Phys. Rev. B **98**, 201112 (2018).
[12] G. Hautier, A. Miglio, G. Ceder, G.-M. Rignanese, and X. Gonze, Nat. Commun. **4**, 2292 (2013).
[13] S. Su, F. Guojia, L. Chun, X. Sheng, and Z. Xingzhong, Phys. Status Solidi A **203**, 1891 (2006).
[14] S. Ichikawa and I. Terasaki, Phys. Rev. B **68**, 233101 (2003).
[15] K. Itoh and N. Tsuda, Solid State Commun. **109**, 715 (1999).
[16] T. Taniguchi, Y. Nagata, T. Ozawa, M. Sato, Y. Noro, T. Uchida, and H. Samata, J. Alloys Compd. **373**, 67 (2004).
[17] K. Itoh, Y. Yano, and N. Tsuda, J. Phys. Soc. Jpn. **68**, 3022 (1999).
[18] L. K. Lamontagne, G. Laurita, M. Knight, H. Yusuf, J. Hu, R. Seshadri, and K. Page, Inorg. Chem. **56**, 5158 (2017).
[19] V. Voorhees and R. Adams, J. Am. Chem. Soc. **44**, 1397 (1922).
[20] D. Cahen and J. A. Ibers, J. Catal. **31**, 369 (1973).
[21] M. S. Hegde, G. Madras, and K. C. Patil, Acc. Chem. Res. **42**, 704 (2009).
[22] J. A. Kurzman, L. M. Misch, and R. Seshadri, Dalton Trans. **42**, 14653 (2013).
[23] Y. Nishihata, J. Mizuki, T. Akao, H. Tanaka, M. Uenishi, M. Kimura, T. Okamoto, and N. Hamada, Nature **418**, 164 (2002).
[24] J. Li, U. G. Singh, T. D. Schladt, J. K. Stalick, S. L. Scott, and R. Seshadri, Chem. Mater. **20**, 6567 (2008).
[25] C. R. Rajamathi, U. Gupta, N. Kumar, H. Yang, Y. Sun, V. Süß, C. Shekhar, M. Schmidt, H. Blumtritt, P. Werner, B. Yan, S. Parkin, C. Felser, and C. N. R. Rao, Adv. Mater. **29**, 1606202 (2017).
[26] B. Yan, B. Stadtmüller, N. Haag, S. Jakobs, J. Seidel, D. Jungkenn, S. Mathias, M. Cinchetti, M. Aeschlimann, and C. Felser, Nat. Commun. **6**, 10167 (2015).
[27] B. J. Wieder, Y. Kim, A. M. Rappe, and C. L. Kane, Phys. Rev. Lett. **116**, 186402 (2016).
[28] L. M. Schoop, M. N. Ali, C. Straßer, A. Topp, A. Varykhalov, D. Marchenko, V. Duppel, S. S. P. Parkin, B. V. Lotsch, and C. R. Ast, Nat. Commun. **7**, 11696 (2016).
[29] B. Bradlyn, J. Cano, Z. Wang, M. G. Vergniory, C. Felser, R. J. Cava, and B. A. Bernevig, Science **353**, 6299 (2016).
[30] R. Hoffmann, Angew. Chem. Int. Ed. **26**, 846 (1987).
[31] M. L. Doublet, E. Canadell, and M. H. Whangbo, J. Am. Chem. Soc. **116**, 2115 (1994).
[32] G. Li, B. Yan, Z. Wang, and K. Held, Phys. Rev. B **95**, 035102 (2017).
[33] G. Kresse and J. Hafner, Phys. Rev. B **49**, 14251 (1994).
[34] G. Kresse and J. Furthmüller, Phys. Rev. B **54**, 11169 (1996).
[35] G. Kresse and J. Furthmüller, Comput. Mater. Sci. **6**, 15 (1996).
[36] P. Blaha, K. Schwarz, G. Madsen, D. Kvasnicka, and J. Luitz, *WIEN2K: An Augmented Plane Wave and Local Orbitals Program for Calculating Crystal Properties* (Karlheinz Schwarz, 2001).
[37] P. E. Blöchl, Phys. Rev. B **50**, 17953 (1994).
[38] G. Kresse and D. Joubert, Phys. Rev. B **59**, 1758 (1999).
[39] K. Schwarz, P. Blaha, and G. Madsen, Comput. Phys. Commun. **147**, 71 (2002).
[40] J. P. Perdew, K. Burke, and M. Ernzerhof, Phys. Rev. Lett. **77**, 3865 (1996).
[41] S. H. Vosko, L. Wilk, and M. Nusair, Can. J. Phys. **58**, 1200 (1980).
[42] A. V. Krukau, O. A. Vydrov, A. F. Izmaylov, and G. E. Scuseria, J. Chem. Phys. **125**, 224106 (2006).
[43] J. A. Kurzman, M.-S. Miao, and R. Seshadri, J. Phys. Condens. Matter **23**, 465501 (2011).
[44] P. Janthon, S. A. Luo, S. M. Kozlov, F. Vies, J. Limtrakul, D. G. Truhlar, and F. Illas, J. Chem. Theory Comput. **10**, 3832 (2014).

[45] F. Tran, D. Koller, and P. Blaha, Phys. Rev. B **86**, 134406 (2012).

[46] H. J. Monkhorst and J. D. Pack, Phys. Rev. B **13**, 5188 (1976).

[47] M. Methfessel and A. T. Paxton, Phys. Rev. B **40**, 3616 (1989).

[48] P. E. Blöchl, O. Jepsen, and O. K. Andersen, Phys. Rev. B **49**, 16223 (1994).

[49] See Supplemental Material at [URL will be inserted by publisher] for comparisons between electronic structure in VASP, WIEN2k, and our tight-binding model, density of states calculations, and additional comparisons between the B_+ and B_- bands described in the text for both the platinum and palladium compound, with and without SOC.

[50] R. V. Panin, N. R. Khasanova, A. M. Abakumov, E. V. Antipov, G. V. Tendeloo, and W. Schnelle, J. Solid State Chem. **180**, 1566 (2007).

[51] J. Waser and E. D. McClanahan, Experientia **6**, 379 (1950).

[52] A. A. Mostofi, J. R. Yates, G. Pizzi, Y.-S. Lee, I. Souza, D. Vanderbilt, and N. Marzari, Comput. Phys. Commun. **185**, 2309 (2014).

[53] Q. Wu, S. Zhang, H.-F. Song, M. Troyer, and A. A. Soluyanov, Comput. Phys. Commun. **224**, 405 (2018).

[54] K. Momma and F. Izumi, J. Appl. Crystallogr. **44**, 1272 (2011).

[55] G. F. Koster, J. O. Dimmock, R. G. Wheeler, and H. Statz, *Properties of the thirty-two point groups*, Dover Books on Chemistry (M.I.T. Press, Cambridge, Massachusetts, 1963).

[56] D. Cahen, J. A. Ibers, and J. B. Wagner, Inorg. Chem. **13**, 1377 (1974).

[57] W. Weber, G. Graham, A. Chen, K. Hass, and B. Chamberland, Solid State Commun. **106**, 95 (1998).

[58] P. L. Smallwood, M. D. Smith, and H.-C. zur Loye, J. Cryst. Growth **216**, 299 (2000).

[59] H. Samata, S. Tanaka, S. Mizusaki, Y. Nagata, T. C. Ozawa, A. Sato, and K. Kosuda, J. Cryst. Process Technol. **2**, 16 (2012).

[60] S. Pezzini, M. R. van Delft, L. M. Schoop, B. V. Lotsch, A. Carrington, M. I. Katsnelson, N. E. Hussey, and S. Wiedmann, Nat. Phys. **14**, 178 (2017).

[61] J. Hu, Z. Tang, J. Liu, X. Liu, Y. Zhu, D. Graf, K. Myhro, S. Tran, C. N. Lau, J. Wei, and Z. Mao, Phys. Rev. Lett. **117**, 016602 (2016).

[62] S. Klemenz, S. Lei, and L. M. Schoop, ArXiv e-prints (2018), arXiv:1808.06619 [cond-mat.mtrl-sci].

Supporting Figures—Fermi level Dirac crossings in 4d and 5d cubic metal oxides: $NaPd_3Q$ and $NaPt_3Q$

Samuel M. L. Teicher[1], Leo K. Lamontagne[1], Leslie M. Schoop,[2] and Ram Seshadri[1]

[1]*Materials Department and Materials Research Laboratory,*

University of California, Santa Barbara 93106, USA and

[2]*Department of Chemistry, Princeton University, Princeton 08540, USA*[*]

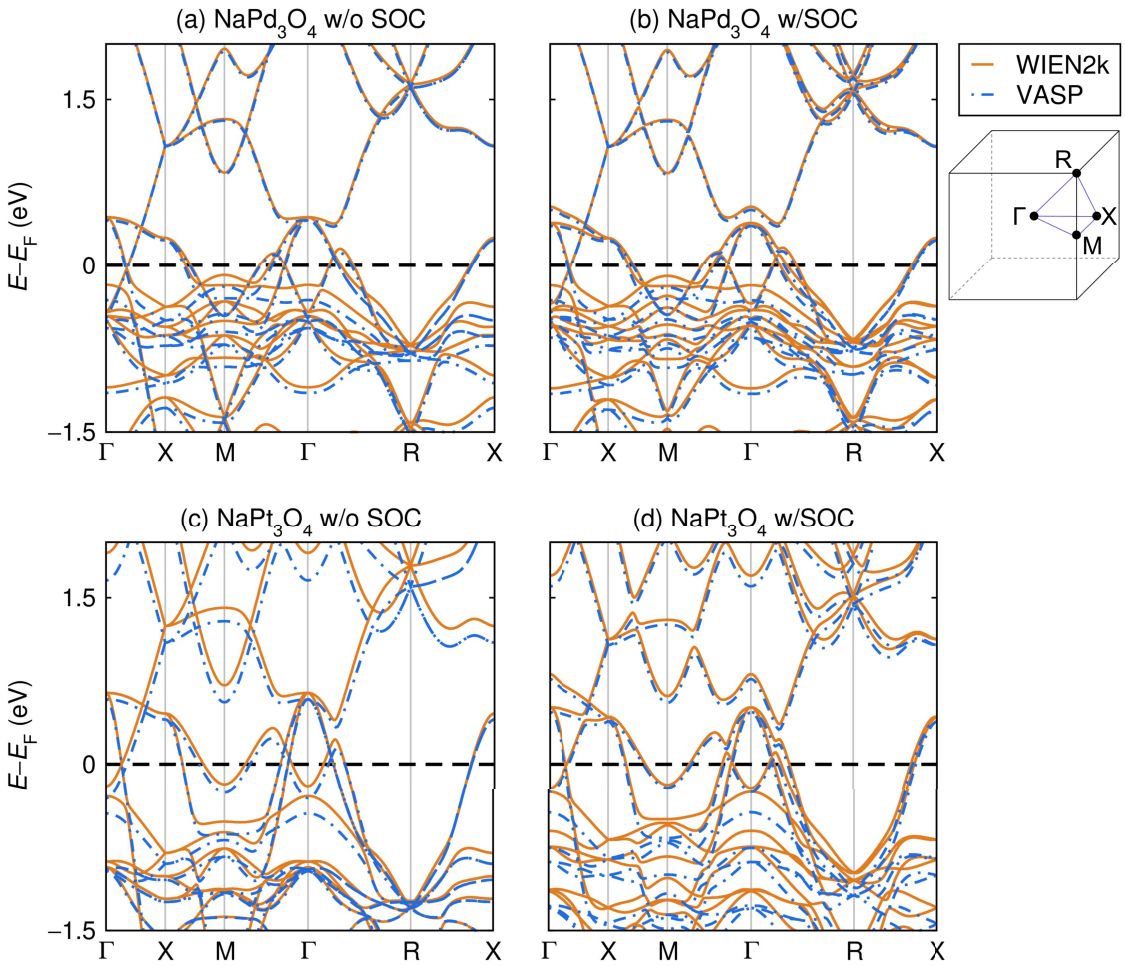

FIG. 1. Comparison of band structures calculated using the DFT codes VASP and WIEN2k. There is good qualitative and quantitative matching between the band structures calculated with both codes above the Fermi level and in the region immediately about the Fermi level in which the Dirac crossings discussed in this paper occur. The differences in calculated energies below the Fermi level are unsurprising given the local orbital method adopted in WIEN2k (but not in VASP).

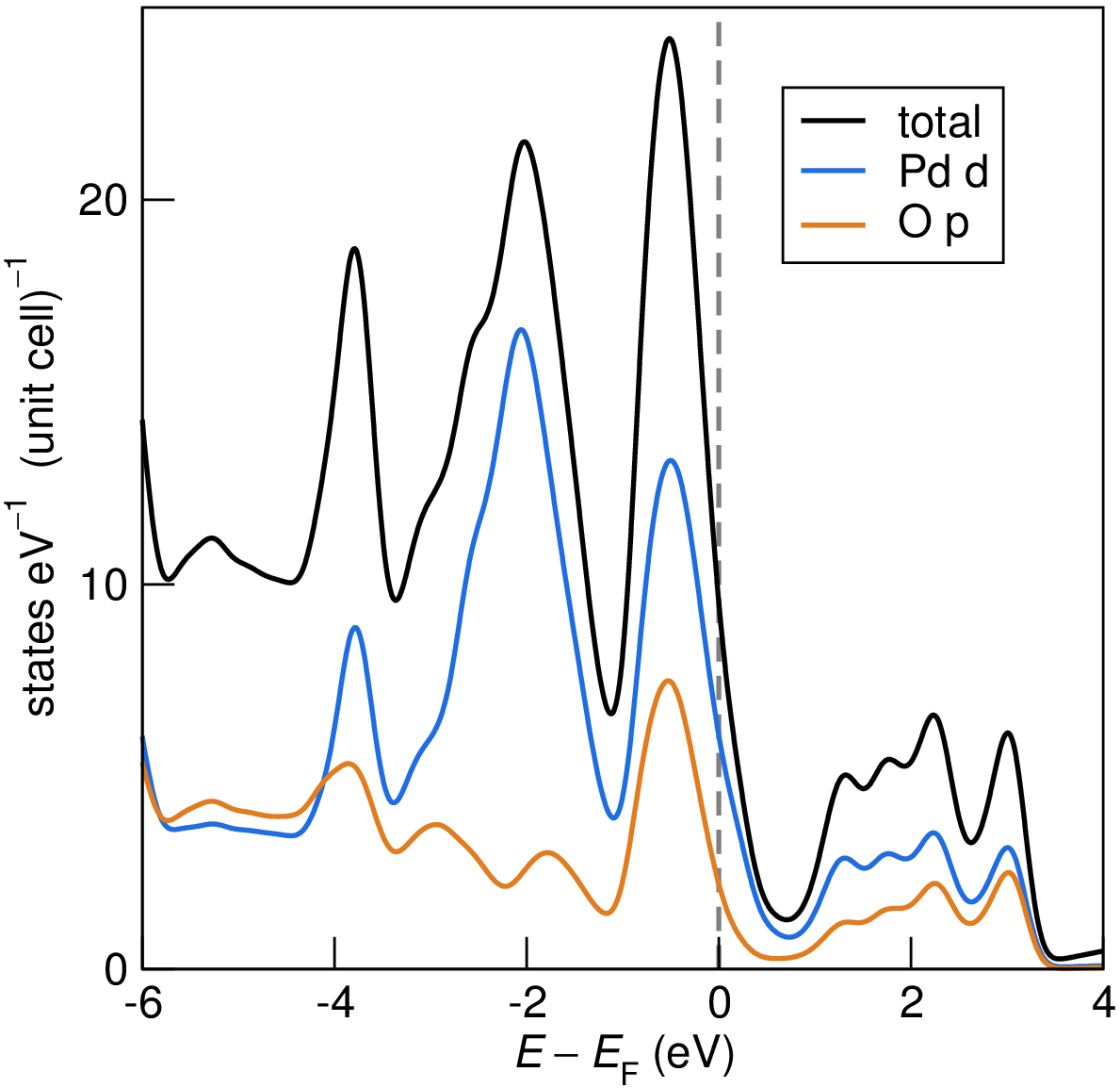

FIG. 2. VASP Density of states (DOS) calculations for $NaPd_3O_4$. Only orbital states contributing to more than 3% of the total DOS are shown. It can be seen that Na states make a negligible contribution near the Fermi level and that the primary contributions to the Fermi level electronic structure come from Pt d and O p states. These results further support the electronic band orbital character assignments made in the body of the paper. Calculations were completed on a $15 \times 15 \times 15$ k-mesh with tetrahedral smearing. A post-calculation Gaussian smoothing was added with a standard deviation of 0.1 eV.

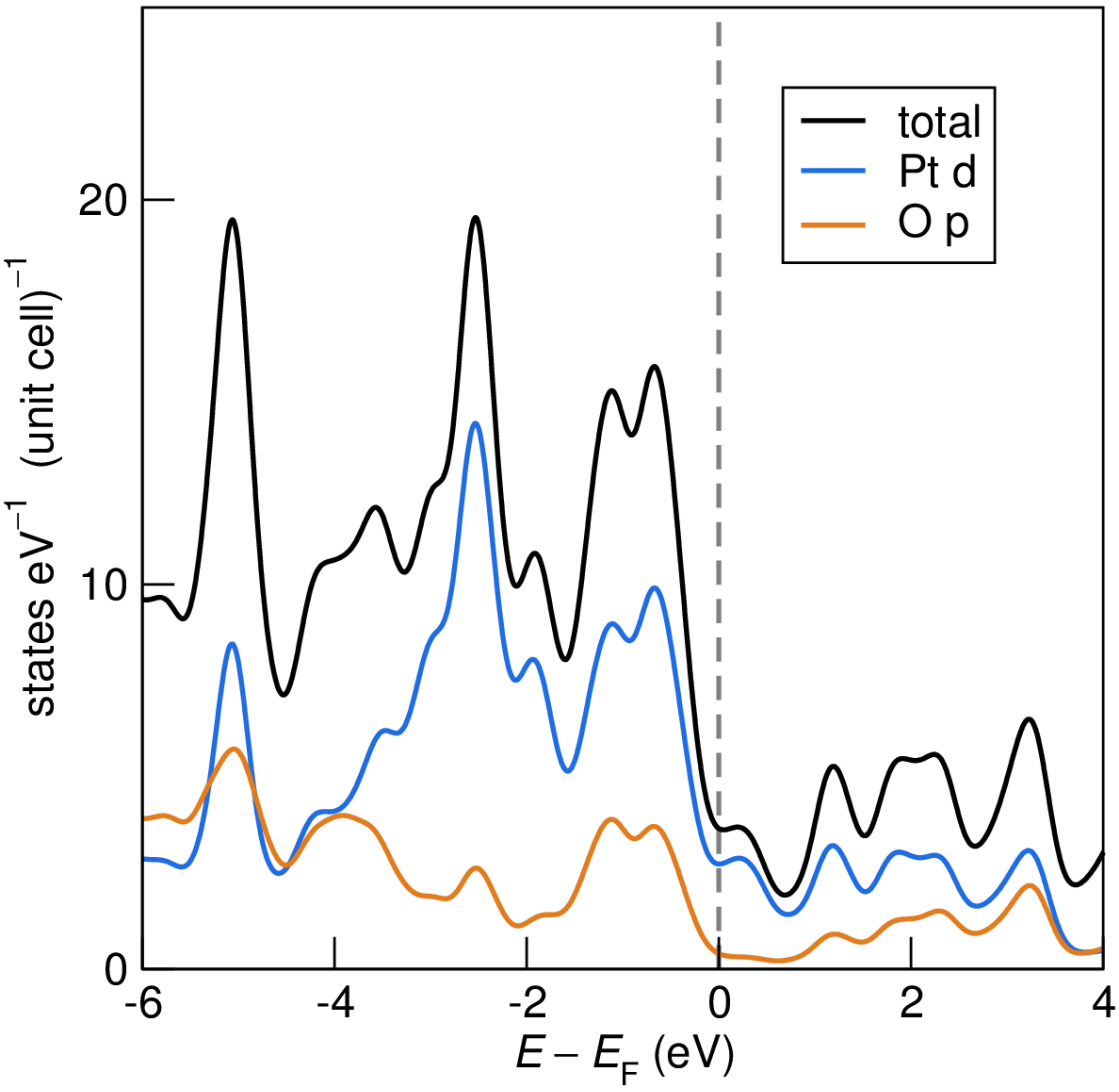

FIG. 3. Density of states (DOS) calculations for $NaPt_3O_4$ calculated in the same manner as the previous figure.

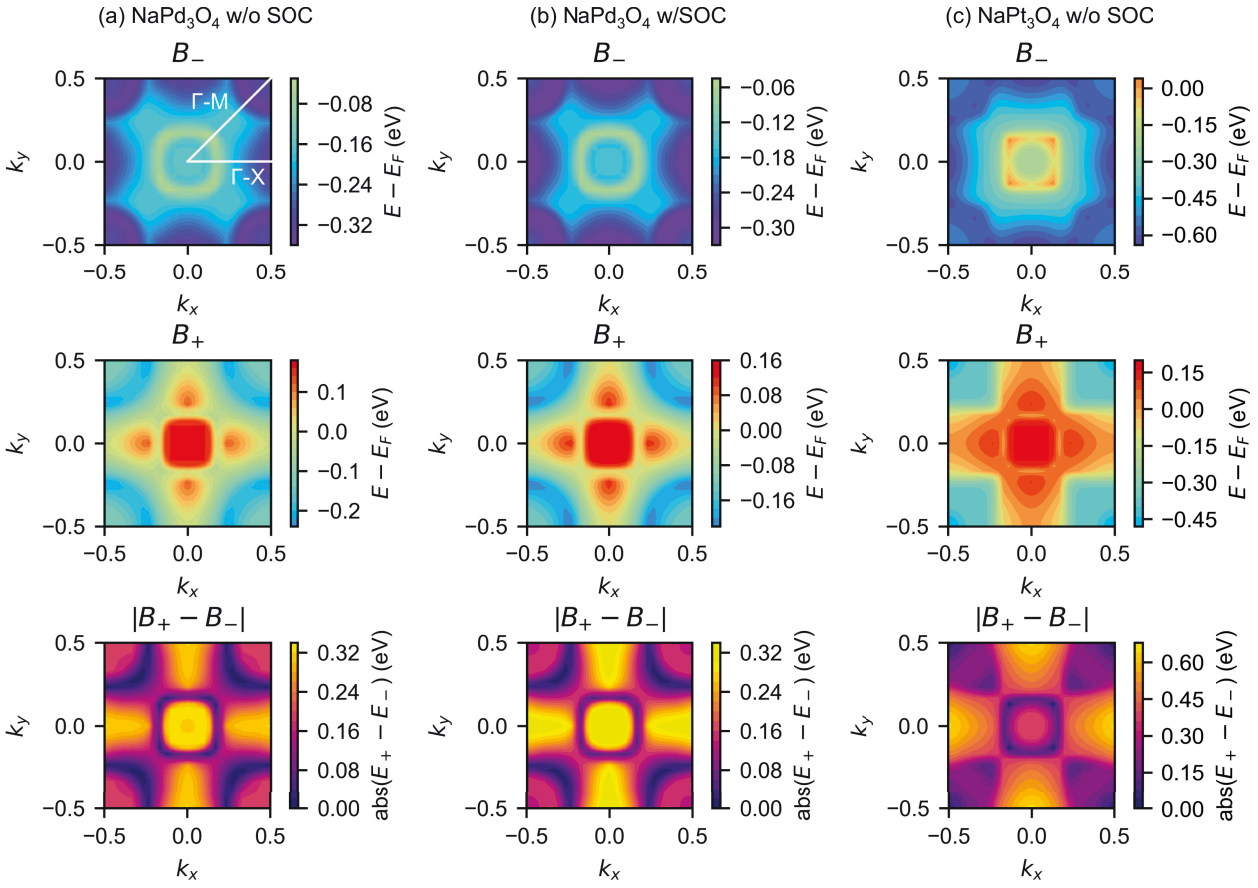

FIG. 4. Heatmaps of band energies on the $k_z = 0$ plane. Energies of the B_- and B_+ bands and the absolute value of the energy separation between these bands are shown for (a) $NaPd_3O_4$ without SOC, (b) $NaPd_3O_4$ with SOC, and (c) $NaPt_3O_4$ without SOC in complement to the calculations for $NaPt_3O_4$ with SOC presented in the body of the paper.

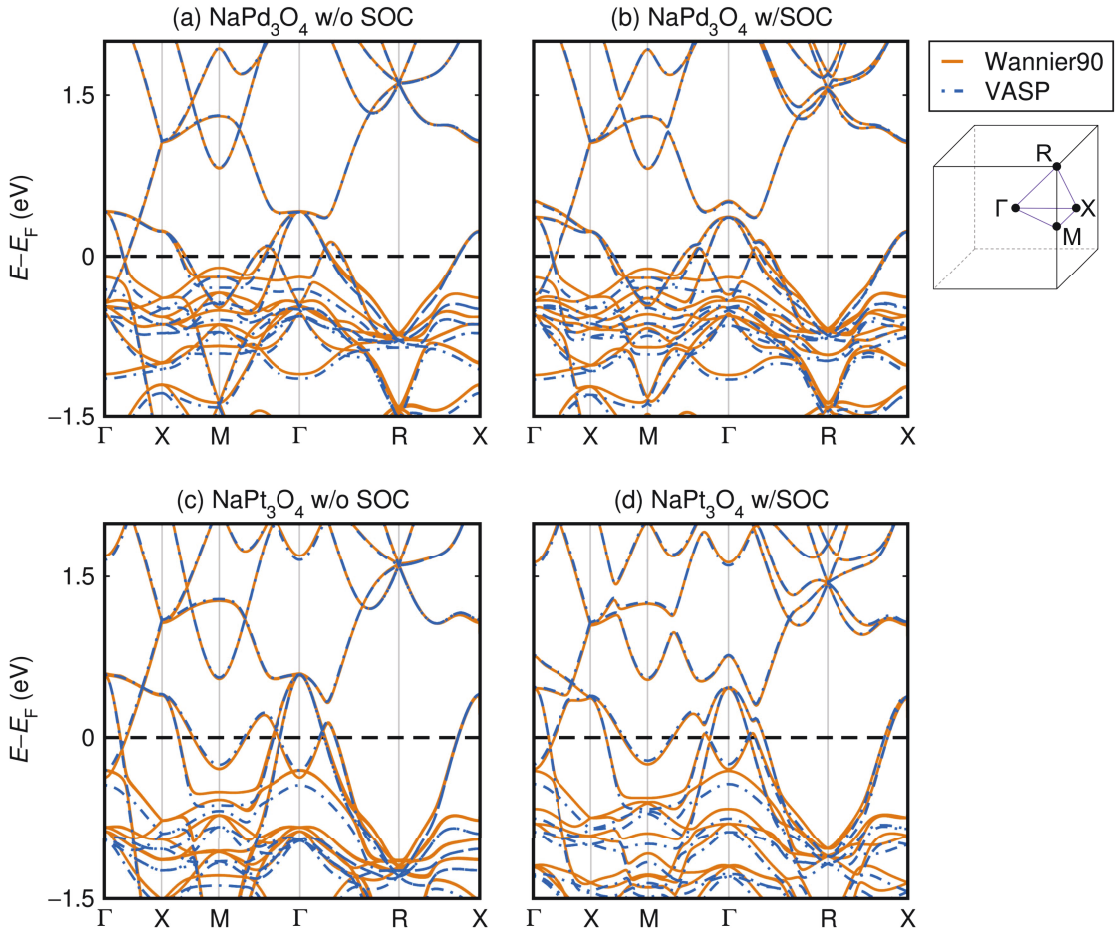

FIG. 5. Comparison of electronic band structures calculated with VASP and via Wannier-interpolation from the Wannier functions fit to our VASP calculations. Excellent agreement can be seen for all states above the Fermi level and in the region near the Fermi level near where the Dirac crossings of interest occur. The orbital-projected Wannier90 band structure does not perfectly match VASP for states far below the Fermi level. Perhaps unsurprisingly, the sub-Fermi level electronic bands determined by Wannier interpolation appear qualitatively similar to those calculated by the local orbital method in WIEN2k. NOTE: The Fermi-level is an externally-provided tuning parameter in these calculations; the Wannier90 band structure Fermi levels have been adjusted by 0.1 eV and 0.25 eV from the VASP calculated values for the Pd and Pt compounds, respectively, in order to visibly overlap with the VASP calculations. Fermi-level ambiguity in the TB calculations is irrelevant to the main results of this paper as we consider only relative energy splittings.

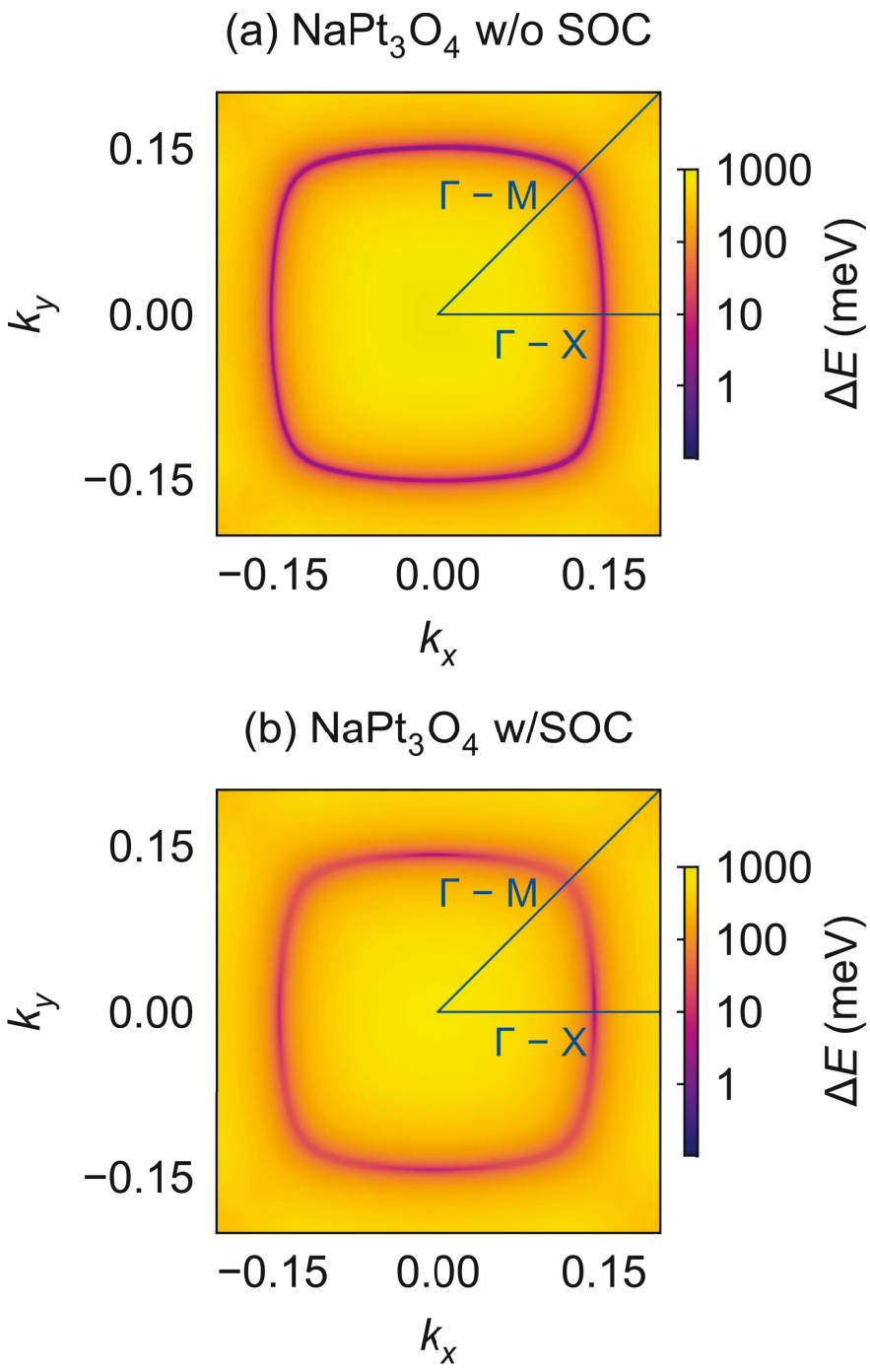

FIG. 6. High resolution plots of B_+/B energy-splitting showing the nodal line on the k_x - k_y plane for (a) $NaPt_3O_4$ without SOC and (b) the gapping of the Dirac degeneracy along -M in $NaPt_3O_4$ with SOC.

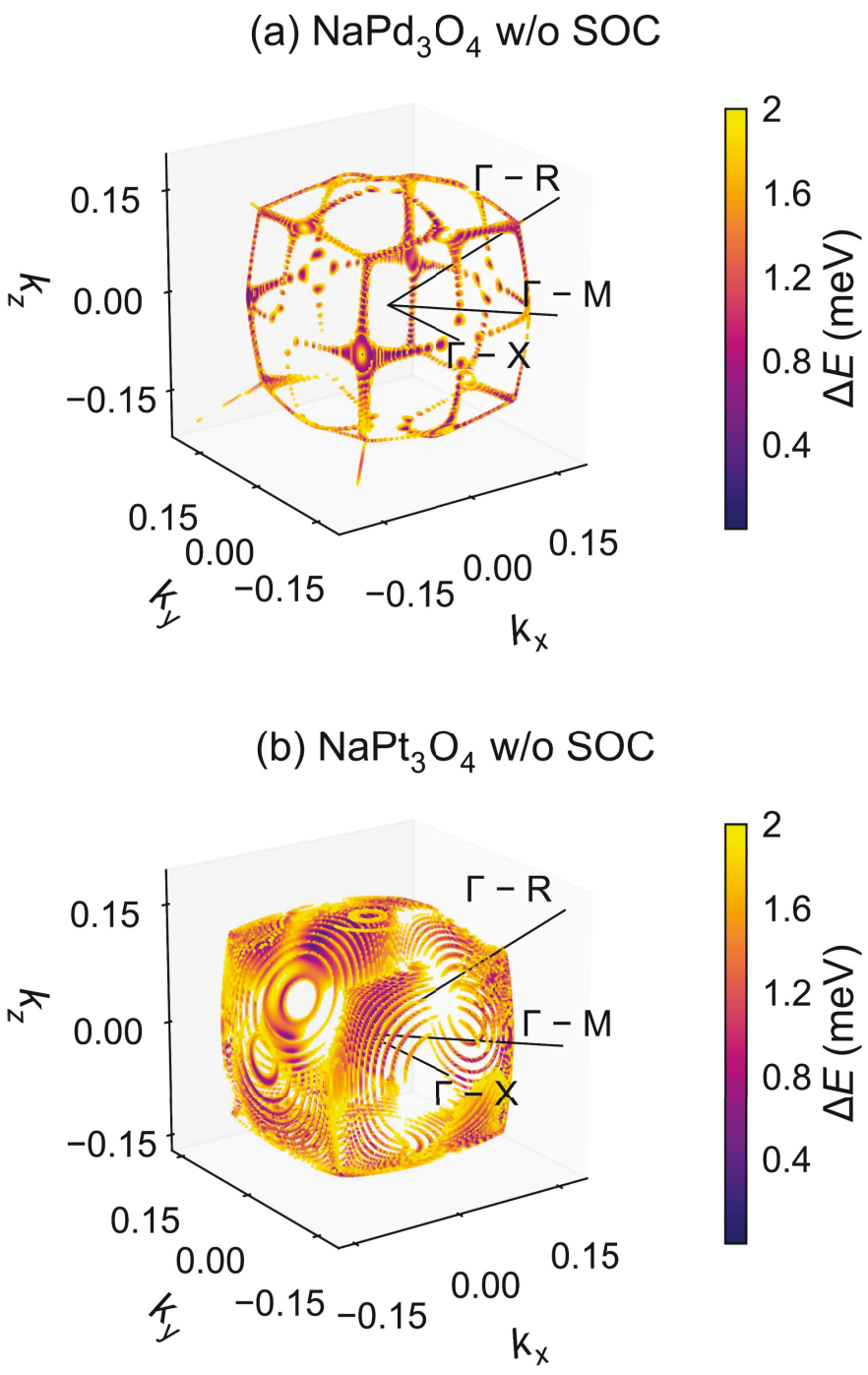

FIG. 7. B_+/B energy-splitting plots with lower energy cutoff for the non-SOC calculations. (a) the smallest energy splittings in the $NaPd_3O_4$ tight-binding model reduce the nodal cube to a series of high-symmetry lines whereas in (b) the $NaPt_3O_4$ Dirac degeneracies form a nodal cube down to the energy resolution of the simulation.

* steicher@ucsb.edu,lschoop@princeton.edu